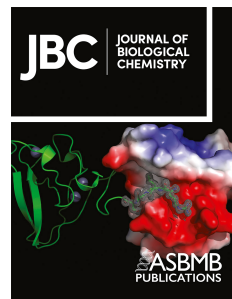


Journal Pre-proof



Titratable transmembrane residues and a hydrophobic plug are essential for manganese import via the *Bacillus anthracis* ABC transporter MntBC-A

Anastasiya Kuznetsova, Gal Masrati, Elena Vigonsky, Nurit Livnat-Levanon, Jessica Rose, Moti Grupper, Adan Baloum, Janet G. Yang, Douglas C. Rees, Nir Ben-Tal, Oded Lewinson

PII: S0021-9258(21)00890-5

DOI: <https://doi.org/10.1016/j.jbc.2021.101087>

Reference: JBC 101087

To appear in: *Journal of Biological Chemistry*

Received Date: 9 February 2021

Revised Date: 12 August 2021

Accepted Date: 16 August 2021

Please cite this article as: Kuznetsova A, Masrati G, Vigonsky E, Livnat-Levanon N, Rose J, Grupper M, Baloum A, Yang JG, Rees DC, Ben-Tal N, Lewinson O, Titratable transmembrane residues and a hydrophobic plug are essential for manganese import via the *Bacillus anthracis* ABC transporter MntBC-A, *Journal of Biological Chemistry* (2021), doi: <https://doi.org/10.1016/j.jbc.2021.101087>.

This is a PDF file of an article that has undergone enhancements after acceptance, such as the addition of a cover page and metadata, and formatting for readability, but it is not yet the definitive version of record. This version will undergo additional copyediting, typesetting and review before it is published in its final form, but we are providing this version to give early visibility of the article. Please note that, during the production process, errors may be discovered which could affect the content, and all legal disclaimers that apply to the journal pertain.

© 2021 THE AUTHORS. Published by Elsevier Inc on behalf of American Society for Biochemistry and Molecular Biology.

Titratable transmembrane residues and a hydrophobic plug are essential for manganese import via the *Bacillus anthracis* ABC transporter MntBC-A

Anastasiya Kuznetsova^{1*}, Gal Masrati^{2*}, Elena Vigonsky¹, Nurit Livnat-Levanon¹, Jessica Rose¹, Moti Grupper³, Adan Baloum¹, Janet G. Yang⁴, Douglas C. Rees⁵, Nir Ben-Tal², and Oded Lewinson¹.

¹Department of Molecular Microbiology and the Rappaport Institute for Medical Sciences, Faculty of Medicine, The Technion-Israel Institute of Technology, Haifa, Israel

²Department of Biochemistry and Molecular Biology, George S. Wise Faculty of Life Sciences, Tel Aviv University, Tel Aviv, Israel.

³Infectious Disease Unit, Rambam Health Care Campus, Haifa, Israel.

⁴Department of Chemistry, University of San Francisco, San Francisco, CA, USA.

⁵Division of Chemistry and Chemical Engineering, California Institute of Technology, Pasadena, CA, USA.

*Equal contribution.

For correspondence: lewinson@technion.ac.il. Telephone number: 972.4.8295408

Running title:

Manganese transport by the virulence-determinant MntBC-A

Statements:

The authors declare no conflict of interests.

The data that support the findings of this study are available from the corresponding author upon reasonable request.

KEYWORDS:

ABC transporter, virulence, transition metals, metal binding, membrane proteins, ATPase.

ABSTRACT

All extant life forms require trace transition metals (*e.g.*, Fe^{2/3+}, Cu^{1/2+}, and Mn²⁺) to survive. However, as these are environmentally scarce, organisms have evolved sophisticated metal uptake machineries. In bacteria, high-affinity import of transition metals is predominantly mediated by ATP-binding cassette (ABC) transporters. During bacterial infection, sequestration of metal by the host further limits the availability of these ions, and accordingly bacterial ABC transporters (importers) of metals are key virulence determinants. However, the structure-function relationships of these metal transporters have not been fully elucidated. Here, we used metal-sensitivity assays, advanced structural modelling, and enzymatic assays to study the ABC transporter MntBC-A, a virulence determinant of the bacterial human pathogen *Bacillus anthracis*. We find that despite its broad metal recognition profile, MntBC-A imports only manganese, whereas zinc can function as a high-affinity inhibitor of MntBC-A. Computational analysis shows that the transmembrane metal permeation pathway is lined with six titratable residues that can coordinate the positively charged metal, and mutagenesis studies show that they are essential for manganese transport. Modelling suggests that access to these titratable residues is blocked by a ladder of hydrophobic residues, and ATP-driven conformational changes open and close this hydrophobic seal to permit metal binding and release. The conservation of this arrangement of titratable and hydrophobic residues among ABC transporters of transition metals suggests a common mechanism. These findings advance our understanding of transmembrane metal recognition and permeation and may aid the design and development of novel antibacterial agents.

INTRODUCTION

Due to the limited chemical reactivity of amino acid side chains, metals such as Cu^{1/2+}, Zn²⁺, Mn²⁺, and Fe^{2/3+} are indispensable cofactors for the structure and function of many enzymes and structural proteins, and it is estimated that metalloproteins comprise 30–40% of most proteomes (1, 2). However, metal ions are also toxic, and therefore all organisms maintain a strict balance between essential uptake and avoiding toxic overload (3). This necessity places trace metals at the crossroads of host-pathogen interactions: to fight infections, hosts employ both metal deprivation and overload in a tissue-specific manner (4–6). In turn, to maintain and control their intracellular metal quota, bacterial pathogens evolved elaborate uptake and extrusion systems (7–9).

For the high-affinity acquisition of essential trace metals, bacteria primarily utilize ATP Binding Cassette (ABC) transporters, and it is therefore not surprising that a large number of ABC transporters (importers) of trace metals have been identified as key bacterial virulence determinants (10–16). ABC transporters comprise one of the largest superfamilies of proteins of any proteome (17, 18). They utilize ATP hydrolysis to transport molecules across biological membranes, and are present in all extant phyla with 79 genes in *E. coli*, ~120 in higher plants, and 48 in human (19). The transported molecules are extremely diverse, ranging from small molecules (such as metal ions, sugars, and amino acids) to large and bulky compounds (peptides, proteins, organo-metal complexes, and antibiotics).

ABC transporters consist minimally of four domains: two transmembrane domains (TMDs) and two cytoplasmic nucleotide-binding domains (NBDs) (20). Binding and hydrolysis of ATP at the NBDs power the translocation of substrates through the permeation pathway formed

by the TMDs. A given ABC transporter may function either as an exporter or an importer. ABC transporters that function as importers depend on a high-affinity substrate binding protein (SBP) that delivers the substrate to the cognate transporter (21–23).

The *mntBCA* operon of the potentially lethal human pathogen *Bacillus anthracis* encodes an ABC import system which has been shown to be an essential virulence determinant: deletion of MntA (hereafter baMntA), the system's SBP, yields a completely non-virulent strain, less virulent than the Sterne strain used for vaccination (10). *In vivo* analysis suggested that baMntBC-A imports manganese and/or iron (10), while *in vitro* studies demonstrated that baMntA does not bind iron but rather binds a variety of other metals, leaving the recognition specificity of the system unclear (24). The mechanism of action of baMntBC-A (or of any other ABC transporter of transition metals) is unknown, and this paucity of information contrasts with their clinical relevance (13, 14, 25–29).

Here, we present a structure-function analysis of the *Bacillus anthracis* transition metal ABC transporter baMntBC-A. Using a combination of experimental and computational approaches, we determined its transport specificity, identified essential transmembrane residues that potentially form a transmembrane metal recognition site, and provide the first description of its ATP hydrolysis cycle.

RESULTS

Transport specificity of baMntBC-A. In a previous study we determined the metal binding spectrum of baMntA of *Bacillus anthracis* (24), the cognate substrate binding protein (SBP) of the baMntBC transporter. We found that baMntA binds several transition metals with affinities ranging from 10^{-6} to 10^{-8} M. The highest affinity was towards Co^{2+} ($K_D \sim 5 \times 10^{-8}$ M), the lowest

towards Ni^{2+} ($K_D \sim 4 \times 10^{-6}$ M) and intermediate binding affinities ($K_D \sim 3-5 \times 10^{-7}$ M) were measured for Mn^{2+} , Zn^{2+} and Cd^{2+} .

Although substrate-binding by the SBP is essential for transport (22, 23, 30, 31), it is not sufficient: several studies have now established that the SBP may bind ligands that are not transported by the transporter (32–34).

To investigate the transport specificity of baMntBC-A, we cloned the coding region of the *Bacillus anthracis mntBCA* transporter and inserted it into an IPTG-inducible *Bacillus subtilis* chromosomal integration vector (35).

We then transformed WT *Bacillus subtilis* with either the empty chromosomal-integration plasmid or with the same plasmid harboring the baMntBC-A transporter. Various metals were added to mid-exponential phase cultures and intracellular metal content was then measured by inductively coupled plasma mass spectroscopy (ICP-MS). We first tested the accumulation of Co^{2+} (added as CoSO_4) since it is the metal that is bound with the highest affinity by baMntA (24), the substrate binding protein of the system. We found that the intracellular concentration of Co^{2+} was independent of the expression of baMntBC-A. Similarly, the intracellular accumulation of Ni^{2+} , Zn^{2+} , and Cd^{2+} was also unchanged upon expression of baMntBC-A (Figure 1A). In contrast, when MnSO_4 was added to the growth media, the intracellular accumulation of Mn^{2+} in cells expressing baMntBC-A was ~2.5-fold higher than in control cells (Figure 1A). Dose-dependent experiments revealed that this fold difference was maintained over a relatively broad range (1–250 μM) of manganese concentrations (Supplementary Figure 1).

These results suggest that despite the broad metal recognition spectrum of the substrate binding protein (MntA) baMntBC-A seems to transport (import) only Mn^{2+} . To confirm that the increased accumulation of manganese is specific to the transport (import)

activity of baMntBC-A we repeated the experiments with a baMntBC-A variant which carries a mutation in the glutamate of the Walker B motif (E163A). In all ABC transporters this conserved glutamate serves as the catalytic base for cleavage of the γ -phosphate bond and is therefore absolutely essential for ATP hydrolysis and transport (20, 36–39). As shown, despite WT-like expression levels of this mutant the intracellular manganese content of cells expressing baMntBC-A (E163A) was identical to that of cells transformed with the control plasmid (Figure 1A, Supplementary Figure 2A). These results suggest that the increased accumulation of manganese in cells expressing WT baMntBC-A is indeed due to the ATPase-dependent transport (import) activity of the transporter.

Time-dependent metal uptake assays revealed that the transport is quite rapid, and significant baMntBC-A-mediated accumulation of manganese was observed in the expressing cells already after 5 min of activity (Figure 1B).

To complement the Mn^{2+} transport assays described above we performed metal-sensitivity growth assays using the previously described manganese-sensitive $\Delta mntR$ *B. subtilis* strain (8)(40). We reasoned that if indeed baMntBC-A functions as a manganese importer its activity will be readily detected in this manganese-sensitive strain. We therefore transformed $\Delta mntR$ cells with either an empty chromosomal-integration plasmid (pDR111) or with the same plasmid that contains the complete baMntBC-A operon under control of the *lac* promoter. As shown in Figure 2A, in the absence of exogenously added manganese, the growth of $\Delta mntR$ *Bacillus subtilis* was not affected by the expression of baMntBC-A, suggesting that the plasmid-driven expression of baMntBC-A is in itself not inhibitory to cell growth. However, even if low concentrations of manganese were added (5 μ M $MnSO_4$) cells that expressed WT baMntBC-A showed a dramatic growth attenuation (Figure 2A). Importantly, cells expressing the inactive variant (E163A) did not

show increased manganese sensitivity. This baMntBC-A-conferred manganese hypersensitivity was observed over a broad range of concentrations (2-160 μ M, Figure 2B). In line with their increased manganese sensitivity, $\Delta mntR$ cells expressing WT baMntBC-A accumulated more manganese than control cells or baMntBC-A (E163A) expressing cells, while their intracellular zinc concentration remained unchanged (Figure 2C).

To complement these studies which were conducted in liquid media, we performed drop-dilution tests in solid media. In line with the results obtained in liquid media, expression of baMntBC-A in the $\Delta mntR$ strain led to increased manganese sensitivity (Figure 2D).

In a previous study (24) we identified three residues that comprise the metal binding site of baMntA: mutations in either H141 or E207 completely abolished manganese recognition, while a mutation in H69 led to ~10-fold reduction in binding affinity. To further substantiate the link between the observed manganese-sensitivity phenotype and expression of functional baMntBC-A we tested the manganese sensitivity of mutants H141A, E207A and H69A.

In the absence of manganese, the growth of $\Delta mntR$ cells expressing these mutants was indiscernible from that of cells expressing WT baMntBC-A or from that of cells transformed with the control plasmid (Figure 3A). In line with their complete inability to bind manganese (24), the manganese-sensitivity of the fully inactive mutants (H141A and E207A) was identical to that of the cells that did not express baMntBC-A (Figure 3B-C), and, as expected, these cells did not over-accumulate manganese (Figure 3D). This lack of activity of mutants H141A and E207A could not be attributed to changes in expression levels caused by the point mutations (Supplementary Figure 2A). Notably, in line with its *in vitro* ~10-fold reduced manganese binding affinity, expression of mutant H69A conferred modest manganese sensitivity, which was significantly different from that of the two fully inactive mutants and from that of the WT protein. ICP-MS analysis revealed that

the intracellular manganese concentration of cells expressing mutants H141A and E207A was comparable to that of cells that did not express baMntBC-A, while the intracellular manganese concentration found in cells expressing mutant H69A was slightly higher (Figure 3D).

Taken together, the results with the four mutations that compromise either the ATPase activity of baMntBC (Figure 2) or manganese binding by baMntA (Figure 3) support the conclusion that the manganese hypersensitivity observed in cells that express WT baMntBC-A is indeed due to active import of manganese by baMntBC-A.

Zn²⁺, but not other metals, inhibits transport of Mn²⁺

In a previous work, we observed that Mn²⁺ and Zn²⁺ compete for binding to the same metal binding site in baMntA (24). In the same work, we also observed that the SBP-Zn⁺² complex is very stable and that Zn²⁺ is released from the SBP at a very slow rate. Although these experiments were conducted in the absence of the transporter, this suggested that Zn²⁺ is a non-transportable metal. Indeed, as shown above (Figure 1A), Mn²⁺ is transported by baMntBC-A while Zn²⁺ is apparently not. Very similar findings were originally reported for PsaA, the Mn²⁺ SBP of *Streptococcus pneumoniae* and therefore the susceptibility of this bacterium to Zn²⁺ was attributed to the Zn²⁺-mediated inhibition of Mn²⁺ uptake (11, 41). Based on these observations it was suggested that Zn²⁺ may be used as an inhibitor of bacterial manganese ABC importers such as baMntBC-A. To test this, we measured the intracellular accumulation of Mn²⁺ in cells that were pre-incubated with Zn²⁺. As shown in Figure 4A, pre-incubating baMntBC-A-expressing cells with Zn²⁺ reduced their intracellular Mn²⁺ content to levels that were similar to those observed in control cells that did not express baMntBC-A. These results suggest that Zn²⁺ inhibits the Mn²⁺ uptake activity of baMntBC-A and therefore may alleviate the manganese hypersensitivity of baMntBC-A- expressing cells.

To test this, we grew control and baMntBC-A-expressing cells in the presence of Mn²⁺, Zn²⁺, and combinations thereof. As shown, addition of 50 μM Zn²⁺ was only marginally inhibitory to growth, and this effect was identical in control and baMntBC-A-expressing cells (Figure 4B, compare orange and blue traces). This is not surprising in light of the lack of Zn²⁺ import activity of baMntBC-A (Figure 1A). As expected, cells expressing baMntBC-A were much more sensitive to the addition of 10 μM Mn²⁺ than control cells (Figure 4B, black symbols). In cells that did not express baMntBC-A, the addition of 50 μM Zn²⁺ on top of 10 μM Mn²⁺ led to a modest (~10%) yet statistically significant greater inhibition (Figure 4B, open red symbols). In contrast, in baMntBC-A-expressing cells, the addition of 50 μM Zn²⁺ on top of 10 μM Mn²⁺ led to ~4-fold higher growth (Figure 4B, full red symbols). These results support the notion that as reported for PsaBCA of *Streptococcus pneumonia* (11, 42), Zn²⁺ inhibits the Mn²⁺ import activity of baMntBC-A. In addition to Mn²⁺ and Zn²⁺, MntA also binds Ni²⁺ and Co²⁺ (24). We therefore tested whether these metals could also serve as MntBC-A inhibitors. Surprisingly, despite its higher binding affinity (~10-fold higher than towards either Mn²⁺ or Zn²⁺, (24)), Co²⁺ had no inhibitory effect, and similar lack of inhibition was also observed with Ni²⁺ (Supplementary Figure 3). The implications and source of the specificity of Zn²⁺ inhibition is discussed later in the manuscript (see discussion).

Model structure of baMntBC and identification of a potential transmembrane metal coordination site.

To gain insight on the structure of baMntBC and its possible transport mechanism we attempted to model it, which proved to be non-trivial. The baMntBC transporter is comprised of two identical subunits of MntC which form the transmembrane domain (TMDs), in complex with two identical subunits of MntB which form the nucleotide binding domain (NBDs). The structure

of the NBDs is highly conserved among the superfamily of ABC transporters (20, 43, 44), and with query-template sequence identity close to 30%, we could use standard homology modeling to model MntB.

Unlike the NBDs, the structure and sequence of the TMDs of ABC transporters can vary significantly (43, 45). Indeed, the modeling of MntC proved to be challenging as only remote homologues are available as templates. Another problem with these templates is that they all transport substrates that are much larger than manganese, making the modeling of the translocation pathway particularly challenging. With sequence identity of only 13%-15% to the available templates, there is uncertainty even regarding the exact number of transmembrane helices. To overcome these challenges, we combined various computational tools to produce multiple model structures of MntC (see Methods). The result of these efforts was three models based on three different templates: (1) *Haemophilus influenza*'s putative molybdate/tungstate importer MolBC in an inward-facing conformation (PDB ID 2NQ2 chains A and B)(46) that resulted in a semi-open MntC model; (2) *Yersinia pestis*'s heme importer HmuUV in an outward-apo conformation (PDB ID 4G1U chains A and B) (47) that resulted in an occluded state model; and (3) *Escherichia coli*'s vitamin B₁₂ importer in an outward-facing AMP-PNP-bound conformation (PDB ID 4R9U chains A and B) (48) that produced an open conformation model. To further assess MntC's model we also produced a template-independent model using trRosetta (49) that predicts inter-residue distance and orientation distributions based on neural networks. Both methods (trRosetta and homology modeling) converged to a similar structure with almost identical assignment of transmembrane helices (Supplementary Figures 4 and 5). Furthermore, all models were consistent with the expected evolutionary conservation pattern, where the protein's core is composed almost exclusively of conserved residues while its periphery is enriched with variable residues

(Supplementary Figure 4 and 5). Nevertheless, due to the low query-to-template sequence identity and the ensuing model uncertainty, in the following structural analysis we considered only features that were observed in all three models irrespective of the template used.

The passage of a charged molecule through a membrane protein often requires coordination by membrane-embedded charged residues that neutralize the translocated charge (chapter 7 in (50)). We hypothesized that this is especially true for transport of manganese, which has one of the highest charge densities of the biologically active divalent metals. Indeed, the model shows six titratable residues that line the trans-membrane translocation cavity (Figure 5A, red spheres), comprised of two triads of Asp 47, His 51, and Asp 94 (DHD), where each triad is contributed by a different monomer of MntC. These three residues are highly conserved among the 430 baMntC homologues we analyzed (Supplementary Figure 6) with a score of 9 in ConSurf's evolutionary conservation scale (1 being the most variable and 9 the most conserved, (51)). Interestingly, none of these residues is conserved in any of the templates used for the modelling and to the best of our knowledge in any other subgroup of ABC transporters. In addition, Asp and His residues are among the most common manganese-coordinating residues (52). Considering the preferred coordination number of 5-6 for manganese (52), the two DHD triads could provide a possible manganese coordination site. Of note, His and Asp residues were demonstrated to directly coordinate binding of Mn²⁺ by baMntA, the system's SBP (24).

To test if residues Asp 47, His 51, and Asp 94 have a role in manganese transport we generated mutants with alanine substitutions of these three putative metal-binding residues. Of note, since MntBC is a hetero-dimer of homodimers, a single substitution at the gene level results in two identical amino acid mutations at the protein level. Next, we compared the activity of these single alanine mutants to that of WT baMntBC using the Mn²⁺ sensitivity assay described above.

As shown in Figure 5B, in the absence of manganese the growth of control cells, cells expressing WT baMntBC or the tested mutants was indistinguishable. In the presence of manganese (Figure 5C), mutations D47A, H51A, and D94A completely abolished the baMntBC-A-mediated Mn²⁺ sensitivity, and the growth of these mutants was identical to that of the vector control and to that of the inactive E163A mutant (which carries a mutation in the essential glutamate of the Walker B motif). The lack of activity of the mutants was not due to improper expression, as their membrane-fraction expression was similar to that of the WT protein (Supplementary Figure 2A). These results demonstrate that the titratable residues are essential for Mn²⁺ transport and support the suggestion that they may be involved in transmembrane metal coordination.

The model shown in Figure 5A is based on the structure of the heme transporter HmuUV (47), depicting baMntBC in an occluded conformation. In this conformation, hydrophobic residues (Ile97, F101, F105, Ile109, and Ile112) from TM helices 5 and 5' form a “hydrophobic ladder” which effectively seals the metal binding site to the extracellular side of the membrane (Figure 5A, blue spheres). Interestingly, the other two models (based on apo MolBC and AMP-PNP-bound BtuCD) depict baMntBC in intermediate stages of opening towards the extracellular environment, where the width of the narrowest point in the hydrophobic seal increases from 3.6 Å (occluded) to 5.4 Å (semi-open), and finally to 11.3 Å (fully-open, top views in Figure 5A, as indicated). To test if the bulky residues that comprise the hydrophobic seal are important for transport, we generated single point glycine substitutions. Glycine was chosen since it is the smallest amino acid. Remarkably, replacement of any of the bulky hydrophobic seal residue with glycine completely abolished the activity of baMntBC (Figure 5D-E), despite normal membrane-fraction expression of the mutants (Supplementary Figure 2B). The relative motions of the residues that comprise the

hydrophobic seal and of those that comprise the charged triads are expected to play an important role in the transport mechanism, as will be discussed later.

Of note, according to all 3-D models, the TMDs of baMntBC are comprised of 9 TM helices per monomer (Figure 5A, supplementary Figure 4), in contrast to the 10 TM helices observed in all crystal structures of baMntBC homologues (46–48). The suggestion that the number of baMntBC TM helices differs from 10 is also supported by all of the transmembrane prediction tools we tested (Supplementary Figure 6). Furthermore, all three homology models of baMntBC, as well as the trRosetta template-free model, show an elongated C-terminal TM helix that extends well into the cytoplasm (Figure 5A). Given that both the N- and C-termini were modeled using an *ab initio* approach (see Material and Methods) the quality of the model in these regions is questionable. Nevertheless, the amino acids composition of the C-terminus is not amphipathic (Supplementary Figure 7) and therefore not expected to lie at the membrane-cytosol interface. In comparison, the N-terminal TM helix is clearly amphipathic (Supplementary Figure 7) and as depicted in the model is expected to lie at the membrane-extracellular interface (Figure 5A, Supplementary Figures 4-7). Further support for the cytosolic location of the C-terminus helical extension is provided by the fact that out of the 21 amino acids that comprise it, six are titratable and six are polar. The net charge of this helical extension is +5, and its cytoplasmic location would be in line with the “positive inside rule” (53, 54). This charge distribution is very different from that observed in all other predicted TM helices of MntC which are heavily enriched in hydrophobic residues (Supplementary Figures 6 and 7). To test if the cytoplasmic extension of this C-terminal TM helix was important for function we truncated it at the membrane-cytosol interface to generate the MntBC-ΔC mutant. Surprisingly, the truncation did not affect the

membrane-expression of MntBC (Supplementary Figure 2B). However, as judged by manganese-sensitivity assays, the truncated variant was completely inactive (Figure 5D-E, green traces).

Uncoupled ATPase activity of baMntBC.

ABC transporters that function as importers are divided into two subgroups: type-I importers typically import sugars, amino acids, and peptides while type-II systems import organometallic complexes such as heme, siderophores, and vitamin B₁₂ (20, 43, 55, 56). These two subclasses have been shown to operate by very distinct mechanisms. One central distinctive mechanistic feature is the basal rate of ATPase activity and its modulation by the SBP.

In type-I systems, the basal rates of ATP hydrolysis are very low, and these are greatly stimulated (10-30-fold) upon docking of the substrate-loaded SBP (34, 57). In contrast, type-II systems have very high rates of basal ATP hydrolysis that are largely insensitive to substrate loading (47, 58, 59). The extent of substrate-modulation of ATPase activity in transition metal ABC importers such as baMntBC is unknown. To study this phenomenon, we codon-optimized the nucleotide sequence of baMntBC for expression in *E. coli* and synthetically generated codon-optimized coding regions for *mntBC* (Genscript NJ, USA). We then prepared inverted membrane vesicles (60) from cells transformed with an empty control plasmid or with plasmids encoding WT or mutant (E163A) baMntBC. We reasoned that due to the high content of baMntBC in these vesicles (inset in Figure 6A) we may be able to measure its ATPase activity without the need of detergent-mediated extraction/purification with its possible pitfalls (61). Indeed, as shown in Figure 6A, the ATPase activity of baMntBC-inverted membrane vesicles was ~5-fold higher than that of vesicles prepared from control cells that were transformed with an empty control plasmid. To verify that this activity is indeed specific to baMntBC we repeated these experiments with the ATPase deficient mutant

baMntBC (E163A). Despite the high protein content of baMntBC (E163A) vesicles (inset in Figure 6A) their ATPase activity was identical to that of the control vesicles that did not contain any baMntBC (Figure 6A).

We next used the vesicles system to investigate the effects of the substrate binding protein (SBP) on ATP hydrolysis by the transporter. For this, codon-optimized baMntA was overexpressed and purified in *E. coli* as previously described (24) and incorporated into the vesicles' lumen at approximately ~10-fold molar excess over baMntBC (see methods for details). Not only did the SBP not stimulate the ATPase activity of the transporter, its incorporation led to a mild inhibitory effect (Figure 6A). We then repeated these experiments incorporating also manganese into the vesicles' lumen at a 50:10:1 manganese: baMntA: baMntBC molar ratio, and observed a similarly modest inhibitory effect (Figure 6A). Collectively, these results suggest that similar to the type-II ABC importer BtuCD yet unlike the Type-I ABC importers MalFGK, YecSC and HisPQM baMntBC has high basal ATPase activity that is not further stimulated by the SBP:substrate complex (34, 37, 57, 58, 62).

To determine the kinetic rate constants of ATP hydrolysis, we measured the initial rates of activity under a range of ATP concentrations. As shown, at ATP concentrations of 15-1000 μM, the initial rates of ATP hydrolysis were linear for at least 2 minutes (Figure 6B-C). To determine the specific ATPase activity of baMntBC, we subtracted the corresponding activity measured in the control vesicles. The net rates of ATP hydrolysis were then plotted as a function of ATP concentration, and the data were fit using the Michaelis–Menten equation (Figure 6D). Adding the term for the Hill coefficient yielded an $n_{HILL}=1.08$, indicating that the two ATP binding sites of baMntBC do not hydrolyze ATP cooperatively. This differs from the cooperative ATP hydrolysis that was reported for both type-I and type -II ABC importers (*e.g.*, MetNI, HisPQM, MalFGK,

YecSC, and BtuCD) (34, 37, 62, 64, 65). Notably, even in a membrane environment baMntBC has very high rates of uncoupled (absence of substrate and SBP) ATPase activity ($k_{cat} = 1.85 \text{ s}^{-1}$), similar to the SBP:substrate-stimulated ATPase rates reported for type-I importers (57, 62).

CONCLUSIONS

In recent years, it is becoming increasingly clear that manganese plays an important role in host-pathogen interactions. Transport and homeostasis of manganese was shown to be essential for the virulence of key bacterial pathogens, such as *Enterococcus faecalis*, *Staphylococcus aureus*, group A *Streptococcus*, *Acinetobacter baumannii*, *Mycobacterium tuberculosis*, *Streptococcus pneumoniae* and many others (14–16, 25, 66–72).

Herein we determined that baMntBC-A transports only manganese, and not any other of the tested metals. Considering that baMntA is absolutely essential for the virulence of *Bacillus anthracis* (10) this means that the high-affinity acquisition of manganese is a major rate-limiting step in the progression of Anthrax. This observation may have interventional potential as had been reported for PsaA of *Streptococcus pneumoniae* (11). In this respect it is noteworthy that the release-kinetics of the metal from the SBP appear to play an essential role in determining the transport specificity on the one hand, and the inhibitory potential on the other: for both *Streptococcus pneumoniae* PsaA and baMntA it was found that zinc is recognized with a similar affinity as manganese yet is released from the SBP at much slower rate (24, 41). In both cases zinc is not transported and acts as an inhibitor. This strategy of using slow-releasing cognate binders of SBPs as inhibitors may be generally applicable also to inhibition of other ABC transporters.

Nickel and cobalt are also recognized by baMntA, the latter with ~10-fold higher affinity than zinc or manganese. Despite that, neither nickel nor cobalt inhibit manganese import by

baMntBC. This difference likely stems from the preferred coordination number of the metals, as has been elegantly demonstrated for the PsaA of *Streptococcus pneumonia* (41). Manganese, cobalt and nickel all prefer hexa-coordinate ligation, while zinc's preferred coordination number is 4 (73–75). The tetrahedral coordination provided by the metal ligating residues of baMntA optimally satisfies zinc's preferred coordination, while binding of manganese, nickel, and cobalt is less favorable. This leads to an almost irreversible binding of zinc, yet reversible binding of manganese, nickel, and cobalt. This is perhaps also the reason why throughout evolution, amoeba, protozoa, and macrophages use zinc to kill phagocytosed bacteria rather than cobalt or nickel (76, 77). On the other of this prey-predator equation, bacteria employ multiple approaches for evading zinc inhibition of manganese import. For example, MntR, the manganese homeostasis master regulator responds only to manganese, and not to zinc (78). This means that MntA will not be unnecessarily exposed to zinc. In addition, bacteria do not live in a thermodynamic equilibrium reality, but rather under constant pre-equilibrium conditions. In such a shifting reality, the faster k_{on} of manganese binding to MntA relative to zinc (24) may provide selectivity favoring the former.

The closest available structural templates for modelling of baMntBC were all type-II ABC importers, suggesting that baMntBC adopts the type-II fold. Similar conclusions can be drawn from the trRosetta template-independent modelling, which yielded a very similar structure. Additional observations also support the notion that ABC importers of transition metals are related to type-II ABC importers. These include the similarity in their cognate SBPs structures, and the fact that unlike SBPs of type-I systems, SBP of transition metals do not undergo large conformational changes upon ligand binding (79–81). The high uncoupled ATPase activity of baMntBC-A (Figure 6) also suggests a similarity to type-II ABC importers (47, 58, 59). However,

these results need to be interpreted with caution as this ATPase activity was measured in *E. coli* membranes which may lack unknown *B. subtilis* components.

In conclusion, our findings suggest that baMntBC-A and likely other ABC importers of transition metals contain unique motifs of two triads of titratable residues and a hydrophobic plug. We propose that these motifs have evolved specifically for the transmembrane translocation of high density charges. Considering their direct relevance to bacterial virulence and pathogenesis, and the emerging power of single particle cryo-EM analysis, we propose that their structure-function analysis is timely.

MATERIALS AND METHODS

Plasmids: The baMntBC-A operon was amplified by PCR from the genome of *Bacillus anthracis* Volum strain and cloned into pDR111 (BGSC) vector for expression in *Bacillus subtilis*, downstream to IPTG-inducible promoter.

Point mutations were introduced into wild type baMntBC-A by using QuikChange Lightning site-directed mutagenesis kit (Agilent Technologies). Mutations were confirmed by sequencing.

Bacillus subtilis strains:

<i>B. subtilis</i>	Genotype and description	Origin
168	trpC2 (Wild type strain)	BGSC
<i>ΔmntR</i>	mntR::erm trpC2 (Knockout of strain 168 locus BSU24520)	BGSC

Transformation to B. subtilis: To construct *B. subtilis* strains expressing baMntBC-A, a transformation protocol for genomic integration was used. Briefly, a single colony of WT or *ΔmntR* *B. subtilis* were picked from LB plate into transformation buffer containing 1X MC buffer and 1

mM MgSO₄ (10x MC buffer containing 0.62 M K₂HPO₄, 0.38 M KH₂PO₄, 20% (w/v) glucose, 30 mM trisodium citrate, 0.022 mg/ml ferric ammonium citrate, 1% (w/v) casein hydrolysate, and 2% (w/v) potassium glutamate), and incubated at 37 °C for 4.5 hr with shaking. One µg of DNA was added and the sample was further incubated for 1.5 hr at 37 °C. Samples were plated on LB plates supplemented with the 150 µg/ml spectinomycin, and plates were incubated at 37°C overnight. Single colonies were picked, baMntBC-A insertion was verified by PCR, and positive colonies were kept in glycerol stock at -80 °C until use.

Manganese sensitivity assays: *B. subtilis* *ΔmntR* transformed with control (pDR111) or baMntBC-A strains were grown in LB supplemented with 150 µg/ml spectinomycin at 37°C. Cells were diluted to A₆₀₀ of 0.05 and 0.15 mL cultures were grown with 1 mM IPTG in the absence or presence of the indicated metal in an automated plate reader (Infinite M200 Pro; Tecan). All metals were added as sulfate salts unless otherwise indicated. The optical density of the cultures was measured every 10 min for 12 hr. All assays were performed in triplicates. For metal sensitivity assays on solid media, cells were grown overnight on LB supplemented with 150 µg/ml spectinomycin at 37°C. Five dilutions were performed and applied drop- wise (1.5 µl) on top of LB plates with the indicated metal concentrations.

Inductively Coupled Plasma Mass Spectrometry (ICP-MS): Metals were added to mid-exponential phase cultures for 15 min at final concentrations of 50-1000 µM, as indicated (all metals were added as sulfate salts unless otherwise indicated). Cells were then harvested and washed with 1X PBS in the presence of 5 mM EDTA. The pellets were resuspended in 69% HNO₃, and incubated in 100°C dry block until complete evaporation. The remaining dry biomass was resuspended in 3% HNO₃ to yield 5-250 ppm, and the final read was corrected for the dilution factor. All ICP-MS

measurements were performed in biological triplicates using Agilent 7500cx ICP-MS with a dynamic range of 0.1 ppt to 2500 ppm.

Preparation of inverted membrane vesicles: Cell pellets were washed once with 50 mM Tris-HCl pH 7.5, 0.5 M NaCl and resuspended (20% w/v) in 50 mM Tris-HCl pH 7.5, 0.5 M NaCl, 30 µg/ml DNase (Worthington), 1 EDTA-free protease inhibitor cocktail tablet (Roche), 1 mM CaCl₂, 1 mM MgCl₂ and ruptured first by tip-sonication and then using an EmulsiFlex-C3 homogenizer (Avestin) at 12000 psi external pressure. Debris and unbroken cells were removed by centrifugation (10000 x g for 20 min) and the membranes were collected by ultracentrifugation at 135000 x g for 30 min, washed once in 25 mM Tris-HCl, pH 7.5, 0.1 M NaCl, and resuspended in the same buffer to ~ 1 mg/mL.

ATPase assays: ATP hydrolysis was measured using Molecular Probes EnzCheck kit, at 37 °C, in a 96-well format, according to the manufacturer's specifications. To initiate hydrolysis, 5 mM MgCl₂ were injected to a solution containing 15 µg of inverted membrane vesicles in 25 mM Tris-HCl, pH 7.5, 0.1 M NaCl, 50 µM EDTA, and the indicated ATP concentration. Data were fitted using either the Michaelis–Menten equation or its expanded version, which includes also a term for the Hill coefficient:

$$V = V_{\max} \frac{[S]^n}{[S]^n + K_m}$$

where V is the observed hydrolysis rate, V_{\max} is the maximal hydrolysis rate, K_m is the Michaelis–Menten constant, $[S]$ is the concentration of ATP, and n is the Hill coefficient.

baMntBC Modeling:

Searching for structural templates: The amino acid sequences of baMntB and baMntC were used as queries in two independent HHpred (82) searches. For baMntB the best scoring templates included the NBDs of *Haemophilus influenzae*'s putative molybdate/tungstate importer

MolBC in an inward-facing conformation (PDB ID 2NQ2); *Yersinia pestis*'s heme importer HmuUV in an outward-apo conformation (PDB ID 4G1U); and *Escherichia coli*'s vitamin B₁₂ importer BtuCD (PDB ID 4R9U). All three templates showed a 28% sequence identity to baMntB. The best scoring templates for baMntC included the same three templates collected for baMntB, only with much lower sequence identity. Specifically, 14%, 15% and 13% for 2NQ2, 4G1U and 4R9U, respectively.

Sequence search and multiple sequence alignment: ConSurf (51) was used to collect independent sets of homologue sequences for baMntB, baMntC and each of the two domains (NBD and TMD) of the three structural templates. Homologue searching was conducted using HMMER (83) with an E-value of 0.0001, maximal sequence identity of 95% and minimal sequence identity of 15% against the clean UniProt database. 500 sequences that sample the list of homologues were chosen automatically by ConSurf and were aligned using MAFFT (84) with default parameters. Fragmented sequences and sequences that introduced large gaps in the multiple sequence alignment (MSA) were then manually removed and the remaining sequences were re-aligned using MAFFT. The final MSAs contained 410 homologues for baMntB; 430 homologues for baMntC; 374 homologues for 2NQ2's NBD and 434 for its TMD; 355 homologues for 4G1U's NBD and 355 for its TMD; and 370 homologues for 4R9U's NBD and 392 for its TMD.

Next, MAFFT was used to perform profile-to-profile MSA between baMntB/baMntC and each of their three templates. From these MSAs, pairwise alignments between baMntB/baMntC and each template were deduced.

Improving the pairwise alignment between baMntC and its templates: Given the low query-to-template sequence identity between baMntC and its templates, we used evolutionary conservation analysis alongside multiple computational tools to independently assign

transmembrane helices and manually improve our pairwise alignments. Specifically, we used HMMTOP, Phobius, TMHMM, TopGraph (85), MEMSAT-SVM (86), TOPCONS (87), RaptorX (88, 89), and ConSurf (51) (Supplementary Figures 4 and 6). Adjustments were made mainly in the regions of the second and fourth predicted helices (amino acids 40-to-67 and 89-to-115 respectively). The improved pairwise alignments were then used for the modelling process.

Constructing the 3D models: MODELLER 9.18 (90) with default settings was used to produce the 3D models of baMntB. Each model was built using one template. For constructing the 3D models of baMntC each of the three templates identified by HHpred were used alongside an ab initio model produced by RaptorX. The latter was mainly used to model gapped regions such as the N- and C-termini. For each model 100 different structures were produced. A short energy minimization was conducted using GROMACS-5.1 (91) and the AMBER99SB-ILDN force field (92). The model with the predicted lowest energy was then selected.

An additional template-independent model was constructed using trRosetta (49) that models a protein's structure using neural network to predict inter-residue distance and orientation distributions based on coevolution data. Default parameters were used with the no-templates option. The resulting model was subjected to a short energy minimization similar to the homology models. Overall, both trRosetta and the homology modeling converged to similar structures. The main difference between the models was the position of TM-4 relative to the other helices (Supplementary Figure 5A). As such, two (F105 and I109) out of the four residues suggested to compose MntC's hydrophobic ladder face the core of each monomer rather than the interface (Supplementary Figure 5B). The overall RMSD when superimposing trRosetta's model to the three homology models ranged between 4.83 - 5.6 Å (Supplementary Table 1). Importantly, the trRosetta calculations account for evolutionary coupling only within the chain. Thus, coupling

between the two monomers in MntC's structure are not taken into account. This means that any constraints that relate to the translocation pathway situated in the interface between the two monomers are ignored by the trRosetta calculations.

REFERENCES:

1. Andreini C, C. G. L. S. R. A. (2013) MetalPDB: a database of metal sites in biological macromolecular structures. - PubMed - NCBI. *Nucleic Acids Res.* [online] <https://www.ncbi.nlm.nih.gov/pubmed/23155064> (Accessed May 7, 2020)
2. Andreini, C., Banci, L., Bertini, I., and Rosato, A. (2008) Occurrence of copper proteins through the three domains of life: A bioinformatic approach. *J. Proteome Res.* **7**, 209–216
3. Klein, J. S., and Lewinson, O. (2011) Bacterial ATP-driven transporters of transition metals: physiological roles, mechanisms of action, and roles in bacterial virulence. *Metalomics*. **3**, 1098–108
4. Becker, K. W., and Skaar, E. P. (2014) Metal limitation and toxicity at the interface between host and pathogen. *FEMS Microbiol. Rev.* **38**, 1235–1249
5. Kehl-Fie, T. E., and Skaar, E. P. (2010) Nutritional immunity beyond iron: a role for manganese and zinc. *Curr. Opin. Chem. Biol.* **14**, 218–224
6. Diaz-Ochoa, V. E., Jellbauer, S., Klaus, S., and Raffatellu, M. (2014) Transition metal ions at the crossroads of mucosal immunity and microbial pathogenesis. *Front. Cell. Infect. Microbiol.* 10.3389/fcimb.2014.00002
7. Guedon, E., Moore, C. M., Que, Q., Wang, T., Ye, R. W., and Helmann, J. D. (2003) The global transcriptional response of *Bacillus subtilis* to manganese involves the MntR, Fur, TnrA and σB regulons. *Mol. Microbiol.* **49**, 1477–1491

8. Que, Q., and Helmann, J. D. (2000) Manganese homestasis in *Bacillus subtilis* is regulated by MntR, a bifunctional regulator related to the diphtheria toxin repressor family of proteins. *Mol. Microbiol.* **35**, 1454–1468
9. Lewinson, O., Lee, A. T., and Rees, D. C. (2009) A P-type ATPase importer that discriminates between essential and toxic transition metals. *Proc. Natl. Acad. Sci. U. S. A.* **106**, 4677–82
10. Gat, O., Mendelson, I., Chitlaru, T., Ariel, N., Altboum, Z., Levy, H., Weiss, S., Grosfeld, H., Cohen, S., and Shafferman, A. (2005) The solute-binding component of a putative Mn(II) ABC transporter (MntA) is a novel *Bacillus anthracis* virulence determinant. *Mol. Microbiol.* **58**, 533–51
11. McDevitt, C. A., Ogunniyi, A. D., Valkov, E., Lawrence, M. C., Kobe, B., McEwan, A. G., and Paton, J. C. (2011) A Molecular Mechanism for Bacterial Susceptibility to Zinc. *PLoS Pathog.* **7**, e1002357
12. Remy, L., Carrière, M., Derré-Bobillot, A., Martini, C., Sanguinetti, M., and Borezée-Durant, E. (2013) The *Staphylococcus aureus* Opp1 ABC transporter imports nickel and cobalt in zinc-depleted conditions and contributes to virulence. *Mol. Microbiol.* **87**, 730–743
13. Ammendola, S., Pasquali, P., Pistoia, C., Petrucci, P., Petrarca, P., Rotilio, G., and Battistoni, A. (2007) High-Affinity Zn²⁺ Uptake System ZnuABC Is Required for Bacterial Zinc Homeostasis in Intracellular Environments and Contributes to the Virulence of *Salmonella enterica*. *Infect. Immun.* **75**, 5867–5876
14. Bearden, S. W., and Perry, R. D. (1999) The Yfe system of *Yersinia pestis* transports iron and manganese and is required for full virulence of plague. *Mol. Microbiol.* **32**, 403–414

15. Janulczyk, R., Ricci, S., and Björck, L. (2003) MtsABC is important for manganese and iron transport, oxidative stress resistance, and virulence of *Streptococcus pyogenes*. *Infect. Immun.* **71**, 2656–2664
16. Paik, S., Brown, A., Munro, C. L., Cornelissen, C. N., and Kitten, T. (2003) The sloABCR operon of *Streptococcus mutans* encodes an Mn and Fe transport system required for endocarditis virulence and its Mn-dependent repressor. *J. Bacteriol.* **185**, 5967–5975
17. Higgins, C. F. (1992) ABC transporters: from microorganisms to man. *Annu. Rev. Cell Biol.* **8**, 67–113
18. Holland, I. B., Cole, S. P. C., Kuchler, K., and Higgins, C. F. (2003) ABC proteins: From Bacteria to Man
19. Dean, M., and Allikmets, R. (2001) Complete Characterization of the Human ABC Gene Family. *J. Bioenerg. Biomembr.* **33**, 475–479
20. Rees, D. C., Johnson, E., and Lewinson, O. (2009) ABC transporters: the power to change. *Nat. Rev. Mol. Cell Biol.* **10**, 218–227
21. Ames, G. F., Mimura, C. S., Holbrook, S. R., and Shyamala, V. (1992) Traffic ATPases: a superfamily of transport proteins operating from *Escherichia coli* to humans. *Adv Enzym. Relat Areas Mol Biol.* **65**, 1–47
22. Schneider, E., Eckey, V., Weidlich, D., Wiesemann, N., Vahedi-Faridi, A., Thaben, P., and Saenger, W. (2012) Receptor-transporter interactions of canonical ATP-binding cassette import systems in prokaryotes. *Eur. J. Cell Biol.* **91**, 311–7
23. Scheepers, G. H., Lycklama a Nijeholt, J. A., and Poolman, B. (2016) An updated structural classification of substrate-binding proteins. *FEBS Lett.* **590**, 4393–4401
24. Vigonsky, E., Fish, I., Livnat-Levanon, N., Ovcharenko, E., Ben-Tal, N., and Lewinson,

- O. (2015) Metal binding spectrum and model structure of the *Bacillus anthracis* virulence determinant MntA. *Metallomics*. **7**, 1407–19
25. Rodriguez, G. M., and Smith, I. (2006) Identification of an ABC Transporter Required for Iron Acquisition and Virulence in *Mycobacterium tuberculosis*. *J. Bacteriol.* **188**, 424–430
26. Marra, A., Lawson, S., Asundi, J. S., Brigham, D., and Hromockyj, A. E. (2002) In vivo characterization of the *psa* genes from *Streptococcus pneumoniae* in multiple models of infection. *Microbiology*. **148**, 1483–91
27. Dintilhac, A., and Claverys, J. P. (1997) The *adc* locus, which affects competence for genetic transformation in *Streptococcus pneumoniae*, encodes an ABC transporter with a putative lipoprotein homologous to a family of streptococcal adhesins. *Res. Microbiol.* **148**, 119–31
28. Pattery, T., Hernalsteens, J. P., and De Greve, H. (1999) Identification and molecular characterization of a novel *Salmonella enteritidis* pathogenicity islet encoding an ABC transporter. *Mol. Microbiol.* **33**, 791–805
29. Paik, S., Brown, A., Munro, C. L., Cornelissen, C. N., and Kitten, T. (2003) The *sloABC*R operon of *Streptococcus mutans* encodes an Mn and Fe transport system required for endocarditis virulence and its Mn-dependent repressor. *J. Bacteriol.* **185**, 5967–5975
30. Karpowich, N. K., Huang, H. H., Smith, P. C., and Hunt, J. F. (2003) Crystal structures of the *BtuF* periplasmic-binding protein for vitamin B12 suggest a functionally important reduction in protein mobility upon ligand binding. *J Biol Chem.* **278**, 8429–8434
31. Berntsson, R. P.-A., Smits, S. H. J. J., Schmitt, L., Slotboom, D.-J., and Poolman, B. (2010) A structural classification of substrate-binding proteins. *FEBS Lett.* **584**, 2606–17
32. de Boer, M., Gouridis, G., Vietrov, R., Begg, S. L., Schuurman-Wolters, G. K., Husada,

- F., Eleftheriadis, N., Poolman, B., McDevitt, C. A., and Cordes, T. (2019) Conformational and dynamic plasticity in substrate-binding proteins underlies selective transport in ABC importers. *Elife.* **8**, e44652
33. Gouridis, G., Schuurman-Wolters, G. K., Ploetz, E., Husada, F., Vietrov, R., de Boer, M., Cordes, T., and Poolman, B. (2015) Conformational dynamics in substrate-binding domains influences transport in the ABC importer GlnPQ. *Nat. Struct. Mol. Biol.* **22**, 57–64
34. Sabrialabe, S., Yang, J. G., and Lewinson, O. (2020) Substrate recognition and ATPase activity of the *E. coli* cysteine/cystine ABC transporter YecSC-FliY. *J Biol Chem*
35. Britton, R. A., Eichenberger, P., Gonzalez-Pastor, J. E., Fawcett, P., Monson, R., Losick, R., and Grossman, A. D. (2002) Genome-wide analysis of the stationary-phase sigma factor (Sigma-H) regulon of *Bacillus subtilis*. *J. Bacteriol.* **184**, 4881–4890
36. Smith, P. C., Karpowich, N., Millen, L., Moody, J. E., Rosen, J., Thomas, P. J., and Hunt, J. F. (2002) ATP binding to the motor domain from an ABC transporter drives formation of a nucleotide sandwich dimer. *Mol. Cell.* **10**, 139–49
37. Tal, N., Ovcharenko, E., and Lewinson, O. (2013) A single intact ATPase site of the ABC transporter BtuCD drives 5% transport activity yet supports full in vivo vitamin B12 utilization. *Proc. Natl. Acad. Sci. U. S. A.* **110**, 5434–9
38. Kadaba, N. S., Kaiser, J. T., Johnson, E., Lee, A., and Rees, D. C. (2008) The high-affinity *E. coli* methionine ABC transporter: structure and allosteric regulation. *Science*. **321**, 250–3
39. Doshi, R., Ali, A., Shi, W., Freeman, E. V., Fagg, L. A., and van Veen, H. W. (2013) Molecular disruption of the power stroke in the ATP-binding cassette transport protein

- MsbA. *J. Biol. Chem.* **288**, 6801–13
40. Huang, X., Shin, J. H., Pinochet-Barros, A., Su, T. T., and Helmann, J. D. (2017) *Bacillus subtilis* MntR coordinates the transcriptional regulation of manganese uptake and efflux systems. *Mol. Microbiol.* **103**, 253–268
41. Couñago, R. M., Ween, M. P., Begg, S. L., Bajaj, M., Zuegg, J., O’Mara, M. L., Cooper, M. A., McEwan, A. G., Paton, J. C., Kobe, B., and McDevitt, C. A. (2014) Imperfect coordination chemistry facilitates metal ion release in the Psa permease. *Nat Chem Biol.* **10**, 35–41
42. Jacobsen, F. E., Kazmierczak, K. M., Lisher, J. P., Winkler, M. E., and Giedroc, D. P. (2011) Interplay between manganese and zinc homeostasis in the human pathogen *Streptococcus pneumoniae*. *Metallomics*. **3**, 38–41
43. Lewinson, O., and Livnat-Levanon, N. (2017) Mechanism of Action of ABC Importers: Conservation, Divergence, and Physiological Adaptations. *J. Mol. Biol.* 10.1016/j.jmb.2017.01.010
44. Locher, K. P. (2016) Mechanistic diversity in ATP-binding cassette (ABC) transporters. *Nat. Struct. Mol. Biol.* **23**, 487–93
45. Locher, K. P. (2009) Review. Structure and mechanism of ATP-binding cassette transporters. *Philos. Trans. R. Soc. Lond. B. Biol. Sci.* **364**, 239–45
46. Pinkett, H. W., Lee, A. T., Lum, P., Locher, K. P., and Rees, D. C. (2007) An inward-facing conformation of a putative metal-chelate-type ABC transporter. *Science*. **315**, 373–7
47. Woo, J.-S., Zeltina, A., Goetz, B. A., and Locher, K. P. (2012) X-ray structure of the *Yersinia pestis* heme transporter HmuUV. *Nat. Struct. Mol. Biol.* **19**, 1310–5

48. Korkhov, V. M., Mireku, S. A., Veprintsev, D. B., and Locher, K. P. (2014) Structure of AMP-PNP-bound BtuCD and mechanism of ATP-powered vitamin B12 transport by BtuCD-F. *Nat. Struct. Mol. Biol.* **21**, 1097–9
49. Yang, J., Anishchenko, I., Park, H., Peng, Z., Ovchinnikov, S., and Baker, D. (2020) Improved protein structure prediction using predicted interresidue orientations. *Proc. Natl. Acad. Sci. U. S. A.* **117**, 1496–1503
50. Kessel, A., and Ben-Tal, N. (2018) *Introduction to Proteins: Structure, Function, and Motion, SECOND EDITION (Chapman & Hall/CRC Mathematical and Computational Biology)*, 2018th Ed., CRC Press
51. Ashkenazy, H., Abadi, S., Martz, E., Chay, O., Mayrose, I., Pupko, T., and Ben-Tal, N. (2016) ConSurf 2016: an improved methodology to estimate and visualize evolutionary conservation in macromolecules. *Nucleic Acids Res.* **44**, W344-50
52. Harding MM (2004) The architecture of metal coordination groups in proteins. *Acta Crystallogr D Biol Crystallogr.* **60(Pt 5)**, 849–59
53. von Heijne, G. (1986) The distribution of positively charged residues in bacterial inner membrane proteins correlates with the trans-membrane topology. *EMBO J.* **5**, 3021–3027
54. Nilsson, J., Persson, B., and Von Heijne, G. (2005) Comparative analysis of amino acid distributions in integral membrane proteins from 107 genomes. *Proteins Struct. Funct. Genet.* **60**, 606–616
55. ter Beek, J., Guskov, A., and Slotboom, D. J. (2014) Structural diversity of ABC transporters. *J. Gen. Physiol.* **143**, 419–35
56. Hollenstein, K., Dawson, R. J., and Locher, K. P. (2007) Structure and mechanism of ABC transporter proteins. *Curr. Opin. Struct. Biol.* **17**, 412–418

57. Davidson, A. L., Shuman, H. A., and Nikaido, H. (1992) Mechanism of maltose transport in *Escherichia coli*: transmembrane signaling by periplasmic binding proteins. *Proc. Natl. Acad. Sci. U. S. A.* **89**, 2360–4
58. Borths, E. L., Poolman, B., Hvorup, R. N., Locher, K. P., and Rees, D. C. (2005) In vitro functional characterization of BtuCD-F, the *Escherichia coli* ABC transporter for vitamin B12 uptake. *Biochemistry*. **44**, 16301–9
59. Vigovsky, E., Ovcharenko, E., and Lewinson, O. (2013) Two molybdate/tungstate ABC transporters that interact very differently with their substrate binding proteins. *Proc. Natl. Acad. Sci. U. S. A.* **110**, 5440–5
60. Reenstra, W. W., Patel, L., Ronald Kaback, H., and Rottenberg, H. (1980) Electrochemical proton gradient in inverted membrane vesicles from *Escherichia coli*. *Biochemistry*. **19**, 1–9
61. Lewinson, O., Orelle, C., and Seeger, M. A. (2020) Structures of ABC transporters: handle with care. *FEBS Lett.* **594**, 3799–3814
62. Liu, C. E., Liu, P. Q., and Ames, G. F. (1997) Characterization of the adenosine triphosphatase activity of the periplasmic histidine permease, a traffic ATPase (ABC transporter). *J. Biol. Chem.* **272**, 21883–91
63. Patzlaff, J. S., van der Heide, T., and Poolman, B. (2003) The ATP/substrate stoichiometry of the ATP-binding cassette (ABC) transporter OpuA. *J. Biol. Chem.* **278**, 29546–51
64. Yang, J. G., and Rees, D. C. (2015) The allosteric regulatory mechanism of the *Escherichia coli* MetNI methionine ATP binding cassette (ABC) transporter. *J. Biol. Chem.* **290**, 9135–40

65. Davidson, A. L., Laghaeian, S. S., and Mannering, D. E. (1996) The maltose transport system of *Escherichia coli* displays positive cooperativity in ATP hydrolysis. *J. Biol. Chem.* **271**, 4858–63
66. Yesilkaya, H., Kadioglu, A., Gingles, N., Alexander, J. E., Mitchell, T. J., and Andrew, P. W. (2000) Role of manganese-containing superoxide dismutase in oxidative stress and virulence of *Streptococcus pneumoniae*. *Infect. Immun.* **68**, 2819–2826
67. Colomer-Winter, C., Flores-Mireles, A. L., Baker, S. P., Frank, K. L., Lynch, A. J. L., Hultgren, S. J., Kitten, T., and Lemos, J. A. (2018) Manganese acquisition is essential for virulence of *Enterococcus faecalis*. *PLoS Pathog.* 10.1371/journal.ppat.1007102
68. Horsburgh, M. J., Wharton, S. J., Cox, A. G., Ingham, E., Peacock, S., and Foster, S. J. (2002) MntR modulates expression of the PerR regulon and superoxide resistance in *Staphylococcus aureus* through control of manganese uptake. *Mol. Microbiol.* **44**, 1269–1286
69. Ando, M., Manabe, Y. C., Converse, P. J., Miyazaki, E., Harrison, R., Murphy, J. R., and Bishai, W. R. (2003) Characterization of the role of the divalent metal ion-dependent transcriptional repressor MntR in the virulence of *Staphylococcus aureus*. *Infect. Immun.* **71**, 2584–2590
70. Turner, A. G., Ong, C. L. Y., Gillen, C. M., Davies, M. R., West, N. P., McEwan, A. G., and Walker, M. J. (2015) Manganese homeostasis in group A *Streptococcus* is critical for resistance to oxidative stress and virulence. *MBio.* 10.1128/mBio.00278-15
71. Juttukonda, L. J., Chazin, W. J., and Skaar, E. P. (2016) *Acinetobacter baumannii* coordinates urea metabolism with metal import to resist host-mediated metal limitation. *MBio.* 10.1128/mBio.01475-16

72. Pandey, R., Russo, R., Ghanny, S., Huang, X., Helmann, J., and Rodriguez, G. M. (2015) MntR(Rv2788): a transcriptional regulator that controls manganese homeostasis in *Mycobacterium tuberculosis*. *Mol. Microbiol.* **98**, 1168–83
73. Irving, D. H., and Williams, R. J. P. *ORDER OF STABILITY OF METAL COMPLEXES*
74. Harding, M. M. (2001) Geometry of metal-ligand interactions in proteins. *Acta Crystallogr. Sect. D Biol. Crystallogr.* **57**, 401–411
75. Harding, M. M. (2002) Metal-ligand geometry relevant to proteins and in proteins: Sodium and potassium. *Acta Crystallogr. Sect. D Biol. Crystallogr.* **58**, 872–874
76. German, N., Doyscher, D., and Rensing, C. (2013) Bacterial killing in macrophages and amoeba: Do they all use a brass dagger? *Future Microbiol.* **8**, 1257–1264
77. Sheldon, J. R., and Skaar, E. P. (2019) Metals as phagocyte antimicrobial effectors. *Curr. Opin. Immunol.* **60**, 1–9
78. Helmann, J. D. (2014) Specificity of metal sensing: Iron and manganese homeostasis in *bacillus subtilis*. *J. Biol. Chem.* **289**, 28112–28120
79. Hsiao, C. D., Sun, Y. J., Rose, J., and Wang, B. C. (1996) The crystal structure of glutamine-binding protein from *Escherichia coli*. *J. Mol. Biol.* **262**, 225–42
80. Sun, Y. J., Rose, J., Wang, B. C., and Hsiao, C. D. (1998) The structure of glutamine-binding protein complexed with glutamine at 1.94 Å resolution: comparisons with other amino acid binding proteins. *J. Mol. Biol.* **278**, 219–29
81. Sharff, A. J., Rodseth, L. E., Spurlino, J. C., and Quiocho, F. A. (1992) Crystallographic evidence of a large ligand-induced hinge-twist motion between the two domains of the maltodextrin binding protein involved in active transport and chemotaxis. *Biochemistry*. **31**, 10657–63

82. Johannes Söding, Andreas Biegert, A. N. L. (2005) The HHpred interactive server for protein homology detection and structure prediction. *Nucleic Acids Res.* [online] <https://www.ncbi.nlm.nih.gov/pmc/articles/PMC1160169/> (Accessed May 13, 2020)
83. Eddy, S. R. (1998) Profile hidden Markov models. *Bioinformatics*. **14**, 755–63
84. Katoh, K., and Standley, D. M. (2013) MAFFT multiple sequence alignment software version 7: Improvements in performance and usability. *Mol. Biol. Evol.* **30**, 772–780
85. Elazar, A., Weinstein, J. J., Prilusky, J., and Fleishman, S. J. (2016) Interplay between hydrophobicity and the positiveinside rule in determining membrane-protein topology. *Proc. Natl. Acad. Sci. U. S. A.* **113**, 10340–10345
86. Nugent, T., and Jones, D. T. (2012) Detecting pore-lining regions in transmembrane protein sequences. *BMC Bioinformatics*. 10.1186/1471-2105-13-169
87. KD.Tsirigos, Peter, C., Shu, N. Käll, L., and Elofsson, A. (2015) The TOPCONS web server for consensus prediction of membrane protein topology and signal peptides. *Nucleic Acids Res.* [online] <https://www.ncbi.nlm.nih.gov/pmc/articles/PMC4489233/> (Accessed May 20, 2020)
88. Wang, S., Sun, S., Li, Z., Zhang, R., and Xu, J. (2017) Accurate De Novo Prediction of Protein Contact Map by Ultra-Deep Learning Model. *PLoS Comput. Biol.* 10.1371/journal.pcbi.1005324
89. Xu, J. (2019) Distance-based protein folding powered by deep learning. *Proc. Natl. Acad. Sci. U. S. A.* **116**, 16856–16865
90. Šali, A., and Blundell, T. L. (1993) Comparative protein modelling by satisfaction of spatial restraints. *J. Mol. Biol.* **234**, 779–815
91. Lindahl, E., Hess, B., and van der Spoel, D. (2001) GROMACS 3.0: A package for

- molecular simulation and trajectory analysis. *J. Mol. Model.* **7**, 306–317
92. Lindorff-Larsen, K., Piana, S., Palmo, K., Maragakis, P., Klepeis, J. L., Dror, R. O., and Shaw, D. E. (2010) Improved side-chain torsion potentials for the Amber ff99SB protein force field. *Proteins Struct. Funct. Bioinforma.* **78**, 1950–1958

ACKNOWLEDGMENTS

This work was supported by grants from NATO Science for Peace and Security Program (SPS 625 Project G4622, OL, NBT), by the US-Israel Binational Science Foundation (BSF grant 2015102 OL, DCR), and by the Israeli Academy of Sciences Project 1006/18 (OL).

AUTHOR CONTRIBUTIONS

EV; Investigation, and Methodology, GM; Data Curation, Formal Analysis, Methodology, NLL; Investigation, Methodology, Supervision, JR, MG, AK, AB; Investigation, Visualization, NBT, OL, JGY, DCR; Supervision, Project Administration, and Funding Acquisition. OL; Conceptualization, Writing Original Draft Preparation. All authors have read and edited the manuscript.

FIGURES

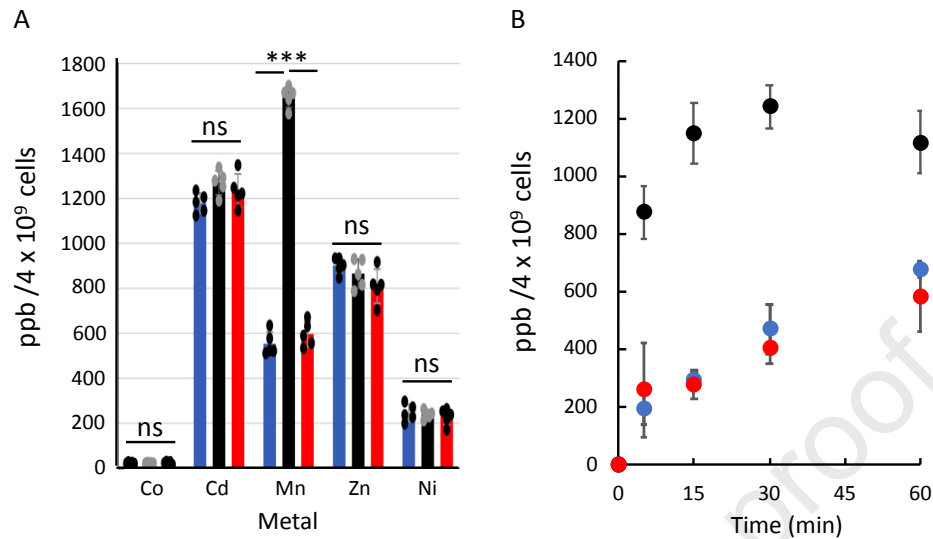


Figure 1. baMntBC-A imports only manganese. (A) Mid exponential phase cultures of *Bacillus subtilis* cells transformed with either a control plasmid (blue bars) or a plasmid encoding WT (black bars) or E163A (red bars) baMntBC-A were incubated for 15 min with 50 μ M of the sulfate salts of the indicated metals. Cells were then harvested, washed with PBS-EDTA buffer, and their intracellular metal content was determined by ICP-MS. Data are mean \pm SDM of replicates ($n=5$). Normal distribution of the data was verified by the Shapiro-Wilk test ($\alpha=0.05$), and statistics were calculated using one-way ANOVA. ***, $p<0.001$; ns, not significant (B) Shown is the time-dependent accumulation of manganese (added at 50 μ M) in control cells (blue circles), or in cells expressing WT (black circles) or E163A (red circles) baMntBC-A.

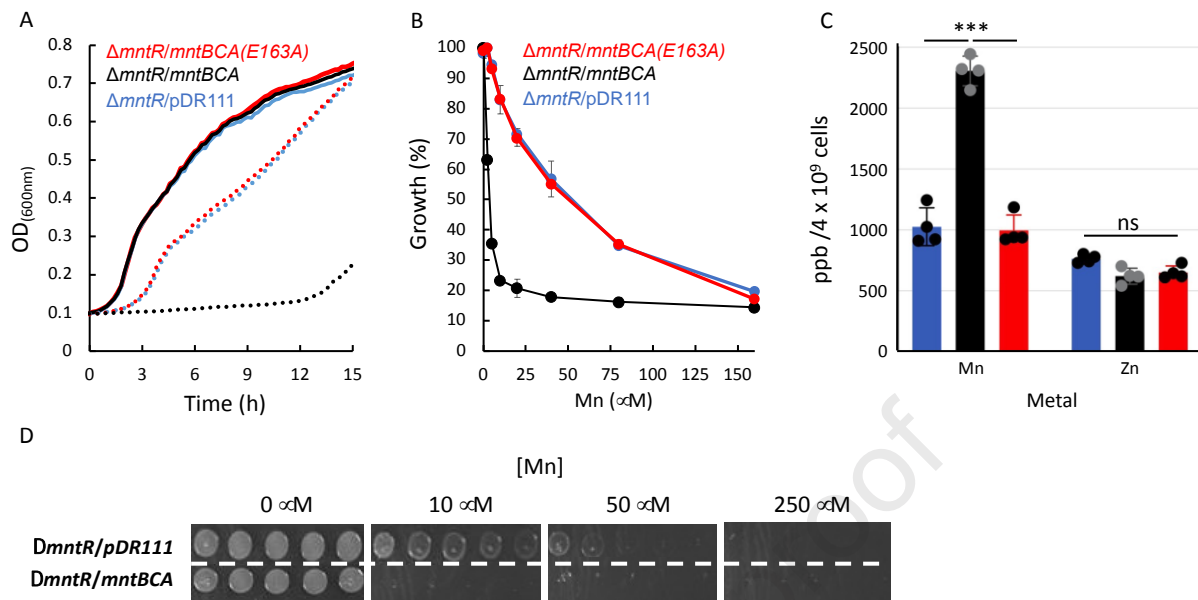


Figure 2. Expression of baMntBC-A leads to increased manganese sensitivity. Cultures of $\Delta mntR$ cells transformed with the pDR111 control plasmid (blue curves) or with the same plasmid encoding WT baMntBC-A (black curves) or the ATPase deficient mutant baMntBC-A (E163A, red curves) were grown in LB media supplemented with IPTG in the absence (solid lines) or presence (dotted lines) of 5 μM MnSO₄. Shown are representative results of experiments conducted at least three times. (B) Cells were grown for 12 h in the presence of the indicated concentration of MnSO₄ and their final OD is expressed as % growth relative to the growth observed in the absence of MnSO₄. Shown are averages of biological triplicates and error bars (shown unless smaller than icons) represent the standard deviations of the mean. (C) Mid exponential phase cultures of $\Delta mntR$ cells transformed with either a control plasmid (blue bars) or a plasmid encoding WT (black bars) or E163A (red bars) baMntBC-A were incubated for 15 min with 50 μM of either MnSO₄ or ZnSO₄ as indicated. Cells were then harvested, washed with PBS-EDTA buffer and their intracellular metal content was determined by ICP-MS. Data are mean \pm SDM of replicates (n=4). Normal distribution of the data was verified by the Shapiro-Wilk test ($\alpha=0.05$), and statistics were calculated using one-way ANOVA. ***, p<0.001; ns, not significant (D) $\Delta mntR$ cells were transformed with a pDR111 control plasmid or with the same plasmid harboring the complete baMntBC-A operon, as indicated. Cultures were grown to mid-exponential phase and then diluted to OD₆₀₀ of 0.01. Drops of 2.5 μL were spotted in serial 10-fold dilutions from left to right onto LB-agar plates supplemented with IPTG in the presence of the indicated concentration of MnSO₄. Shown are representative results of experiments conducted at least three times. The dashed line represents a crop from single unprocessed image.

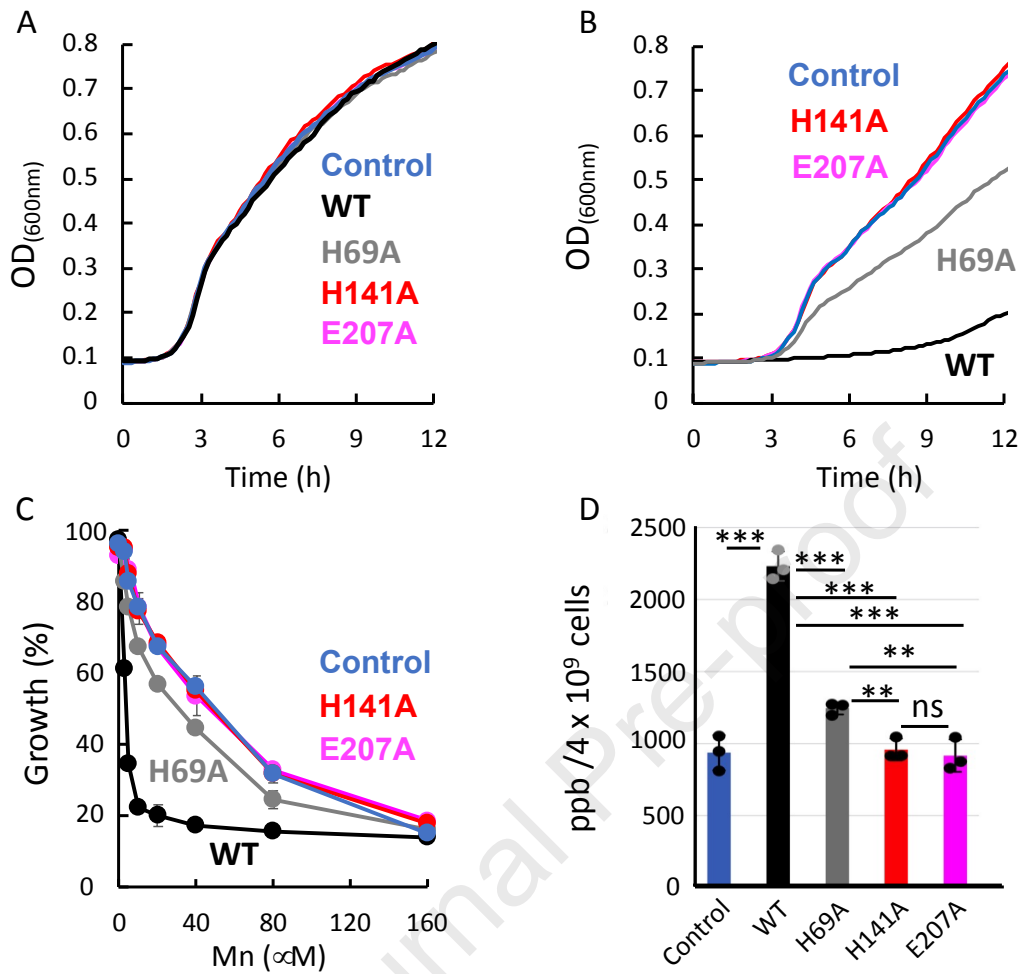


Figure 3. Mutations of the metal binding residues of baMntA abolish the manganese sensitivity.

Cultures of $\Delta mntR$ cells transformed with the pDR111 control plasmid or with the same plasmid encoding WT or mutant baMntBC-A (as color indicated) were grown in LB media supplemented with IPTG in the absence (A) or presence (B) of 5 μ M MnSO₄. Shown are representative results of experiments conducted at least three times. (C) $\Delta mntR$ cells were grown for 12 h in the presence of the indicated concentration of MnSO₄ and their final OD is expressed as % growth relative to the growth observed in the absence of MnSO₄. Shown are averages of biological triplicates and error bars (shown unless smaller than icons) represent the standard deviations of the mean. (D) Mid exponential phase cultures of *Bacillus subtilis* cells transformed with either a control plasmid or with the same plasmid encoding WT or mutant baMntBC-A (as color indicated) were incubated for 15 min with 50 μ M of MnSO₄. Cells were then harvested, washed with PBS-EDTA buffer and their intracellular metal content was determined by ICP-MS. Data are mean \pm SDM of replicates ($n=3$). Normal distribution of the data was verified by the Shapiro-Wilk test ($\alpha=0.05$), and statistics were calculated using one-way ANOVA. ***, $p<0.001$; **, $p<0.05$; ns, not significant.

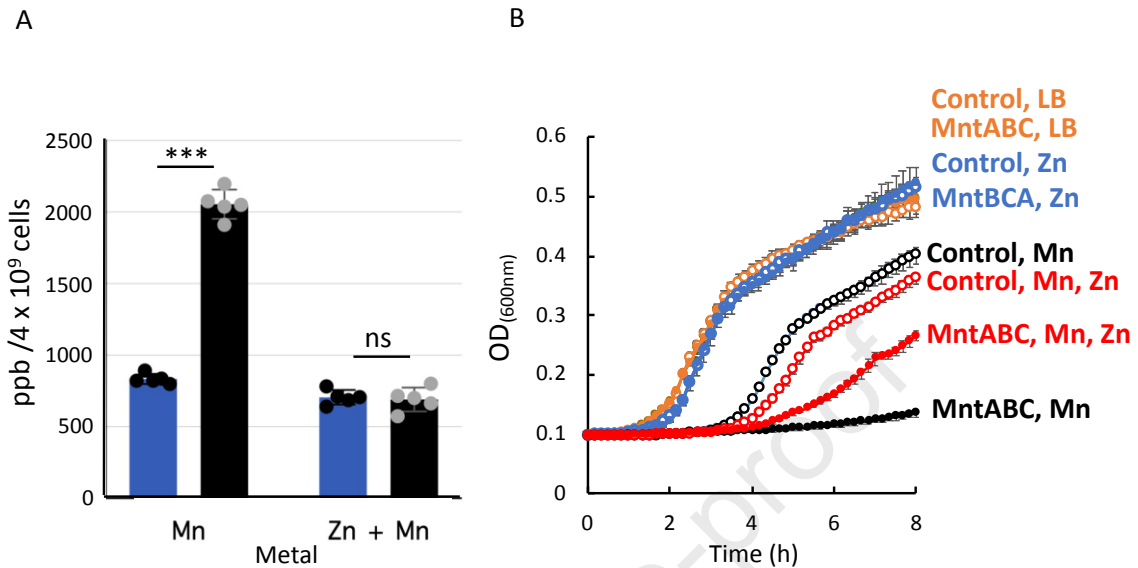


Figure 4. Zinc inhibits baMntBC-A-mediated transport of manganese.

(A) Mid exponential-phase cultures of WT *Bacillus subtilis* 168 cells transformed with either a control plasmid (blue bars) or a plasmid harboring the complete baMntBC-A operon (black bars) were incubated for 15 min with 100 μ M of the indicated metals. Cells were then harvested, washed with PBS-EDTA buffer and the intracellular metal content was determined by ICP-MS. Data are mean \pm SDM of replicates ($n=5$). Normal distribution of the data was verified by the Shapiro-Wilk test ($\alpha=0.05$), and statistics were calculated using one-way ANOVA. ***, $p<0.001$; ns, not significant. (B) Cultures of *Bacillus subtilis* $\Delta mntR$ cells transformed with a control plasmid (open symbols) or a plasmid harboring the complete baMntBC-A operon (full symbols) were grown in LB media (orange symbols) or LB media supplemented with 10 μ M MnSO₄ (black symbols), 50 μ M ZnSO₄ (blue symbols), or their combination (red symbols). Shown are averages of biological triplicates, error bars (shown unless smaller than the symbols) represent standard deviations of the mean.

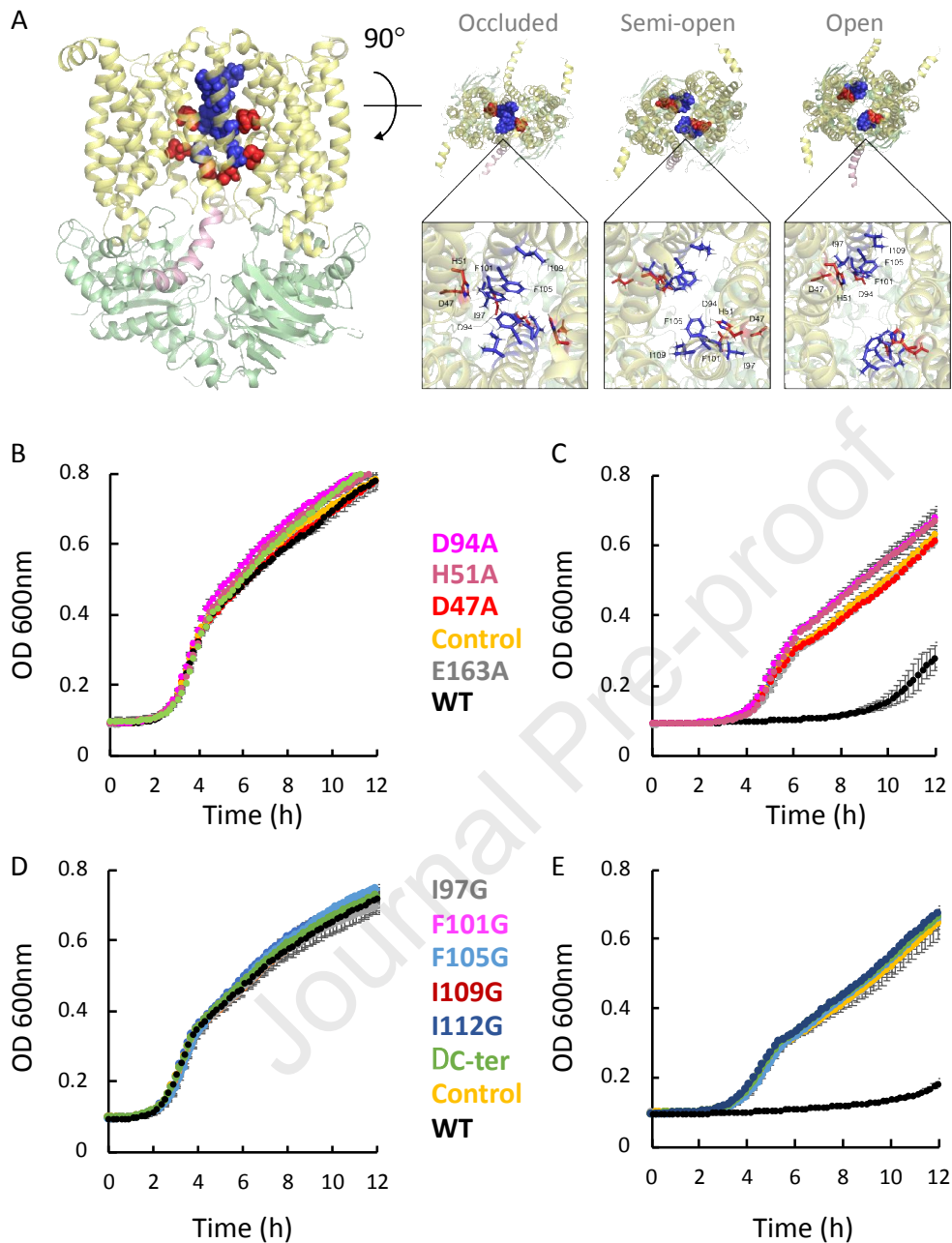


Figure 5. Essential titratable residues line the translocation cavity of baMntBC. (A) Shown are side (left) and top (all other) views of semi-transparent cartoon representations of the baMntBC models. The two left images are of the model that is based on the structure of HmuUV, depicting an occluded conformation. BtuD is colored lime, BtuC in light yellow, and the C-terminal helical extension in salmon pink. The right two images are based on the structures of MolBC and BtuCD and depict a semi-open and open conformations, respectively. Residues of interest are shown either as spheres (full size images) or in sticks representation (zoomed images). The twin charged triads, each composed of Asp 47, His 51, and Asp 94 are shown in red and the “hydrophobic ladder” residues (Ile97, F101, F105, Ile109, and Ile112) are in blue. (B-E) Cultures of Δ mntR cells were grown in the absence (B, D) or presence (C, E) of 10 μ M MnSO₄. In the absence of manganese, WT baMntBC-A and all tested mutants grew similarly. In

the presence of manganese mutations in the putative metal binding residues Asp 47, His 51, and Asp 94 (C) or in hydrophobic seal residues I97, F101, F105, I109, I112 or truncation of the C-terminal helix (E) abolished the activity of baMntBC-A and the growth of these mutants was similar to that of controls cells that did not express baMntBC-A or to that of cells expressing the inactive mutant E163A.

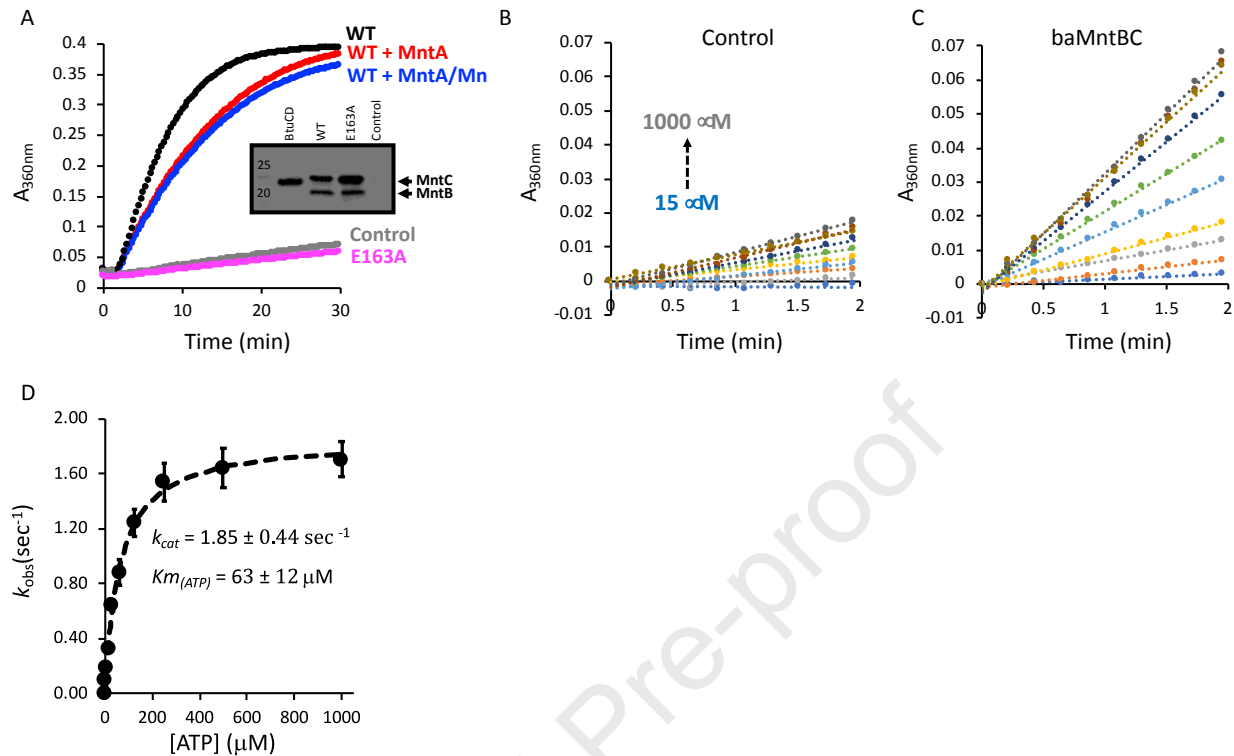


Figure 6. Uncoupled ATP hydrolysis by baMntBC. (A) 15 μg of inverted membrane vesicles were incubated for 2 min with 1mM ATP, and to initiate hydrolysis 2mM MgSO₄ were injected at 2 min. The rate of release of inorganic phosphate was determined by continuous monitoring of the 360 nm absorbance of the solution using the EnzCheck kit. Shown is the activity measured for vesicles containing WT baMntBC (black), WT baMntBC+ baMntA (red), WT baMntBC+ 10 μM baMntA+ 50 μM MnSO₄ (blue), mutant E163A (magenta), or control vesicles (grey). Results are representative of experiments conducted at least three times. The inset shows an immunoblot of SDS page of the vesicles, and BtuCD (used as benchmark for high expression level) and WT or mutant E163A are shown as indicated. (B, C) Initial rates of hydrolysis of 15-1000 μM ATP were measured (in the presence of baMntA and MnSO₄) for control (B) and WT baMntBC (C) vesicles. (D) The initial rates of ATP hydrolysis measured in 'B' for the control vesicles were subtracted from the rates measured for WT baMntBC in 'C'. The net values were plotted as a function of the ATP concentration, and data was then fit using the Michaelis–Menten equation (dashed line). Also shown are mean values ($n=3$) of the kinetic rate constants, error bars represent standard deviations of the mean.

